Article

High-Performance Hole-Transport Layers for Polymer Light-Emitting Diodes. Implementation of Organosiloxane Cross-Linking Chemistry in Polymeric Electroluminescent Devices

He Yan, Paul Lee, Neal R. Armstrong, Amy Graham,
Guennadi A. Evmenenko, Pulak Dutta, and Tobin J. Marks

J. Am. Chem. Soc., **2005**, 127 (9), 3172-3183• DOI: 10.1021/ja044455q • Publication Date (Web): 08 February 2005

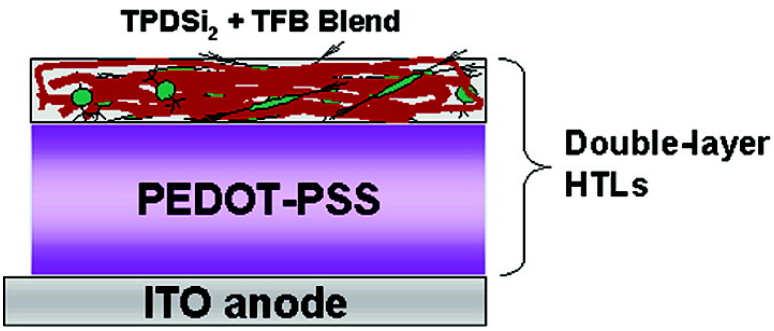

More About This Article

Additional resources and features associated with this article are available within the HTML version:

- Supporting Information
- Links to the 25 articles that cite this article, as of the time of this article download
- Access to high resolution figures
- Links to articles and content related to this article
- Copyright permission to reproduce figures and/or text from this article

View the Full Text HTML

J|A|C|S
ARTICLES
Published on Web 02/08/2005

High-Performance Hole-Transport Layers for Polymer Light-Emitting Diodes. Implementation of Organosiloxane Cross-Linking Chemistry in Polymeric Electroluminescent Devices

He Yan,[†] Paul Lee,[‡] Neal R. Armstrong,[‡] Amy Graham,[‡] Guennadi A. Evmenenko,[§] Pulak Dutta,[§] and Tobin J. Marks*,[†]

Contribution from the Department of Chemistry and the Materials Research Center, Northwestern University, Evanston, Illinois 60208, Department of Chemistry and Optical Science Center, University of Arizona, Tucson, Arizona, 85721, and Department of Physics and Astronomy and the Materials Research Center, Northwestern University, Evanston, Illinois, 60208

Received September 13, 2004; E-mail: t-marks@northwestern.edu

Abstract: This contribution describes an organosiloxane cross-linking approach to robust, efficient, adherent hole-transport layers (HTLs) for polymer light-emitting diodes (PLEDs). An example is 4,4′-bis[(*p*-trichlorosilylpropylphenyl)phenylamino]biphenyl ($TPDSi_2$), which combines the hole-transporting efficiency of *N*,*N*-diphenyl-*N*,*N*-bis(3-methylphenyl)-1,1-biphenyl)-4,4-diamine) (TPD, prototypical small-molecule HTL material) and the strong cross-linking/densification tendencies of organosilanol groups. Covalent chemical bonding of $TPDSi_2$ to PLED anodes (e.g., indium tin oxide, ITO) and its self-cross-linking enable fabrication of three generations of insoluble PLED HTLs: (1) self-assembled monolayers (SAMs) of $TPDSi_2$ on ITO; (2) cross-linked blend networks consisting of $TPDSi_2$ + a hole transporting polymer (e.g., poly(9,9-dioctylfluorene-*co*-N-(4-(3-methylpropyl))diphenylamine), TFB) on ITO; (3) $TPDSi_2$ + TFB blends on ITO substrates precoated with a conventional PLED HTL, poly(3,4-ethylenedioxythiophene)-poly(styrenesulfonate) (PEDOT-PSS). PLED devices fabricated using these new HTLs exhibit comparable or superior performance vs comparable devices based on PEDOT-PSS alone. With these new HTLs, current efficiencies as high as ∼17 cd/A and luminances as high as ∼140,000 cd/m^2 have been achieved. Further experiments demonstrate that not only do these HTLs enhance PLED anode hole injection but they also exhibit significantly greater electron-blocking capacity than PEDOT-PSS. The present organosiloxane HTL approach offers many other attractions such as convenience of fabrication, flexibility in choosing HTL components, and reduced HTL-induced luminescence quenching, and can be applied as a general strategy to enhance PLED performance.

I. Introduction

Impressive scientific and technological progress has recently been achieved in the area of organic light-emitting diodes (OLEDs), motivated by potential applications in a large variety of display technologies. OLEDs are "dual-injection" devices in which holes and electrons are injected from opposite electrodes into an active molecular/macromolecular medium to produce, via exciton decay, light emission.[1−8] OLED responses are usually evaluated with respect to the following characteristics: luminance, light intensity per unit area; turn-on voltage, voltage required for a device to reach luminance of ∼1 cd/m^2; and current efficiency, luminance per unit current density. To achieve optimum device performance, it is desirable to have multilayer structures[9] having discrete-hole transport layer (HTL),[1] emissive layer (EML), and electron-transport layer (ETL)[3] functions. The role of the HTL is not only to maximize hole injection from the anode (usually ITO, tin-doped indium oxide), but also to block efficiency-depleting electron overflow from, and to confine excitons within, the EML.[1,9,10] With such multilayer structures, high-performance devices[11] have been realized for

[†] Department of Chemistry and the Materials Research Center, Northwestern University.
[‡] University of Arizona.
[§] Department of Physics and Astronomy and the Materials Research Center, Northwestern University.

(1) Tang, C. W.; VanSlyke, S. A. *Appl. Phys. Lett.* **1987**, *51*, 913−915.
(2) Burroughes, J. H.; Bradley, D. D. C.; Brown, A. R.; Marks, R. N.; Mackay, K.; Friend, R. H.; Burns, P. L.; Holmes, A. B. *Nature* **1990**, *347*, 539−541.
(3) Brown, A. R.; Bradley, D. D. C.; Burroughes, J. H.; Friend, R. H.; Greenham, N. C.; Burn, P. L.; Holmes, A. B.; Kraft, A. *Appl. Phys. Lett.* **1992**, *61*, 2793−2795.
(4) Baldo, M. A.; Lamansky, S.; Burrows, P. E.; Thompson, M. E.; Forrest, S. R. *Appl. Phys. Lett.* **1999**, *75*, 4−6.
(5) Friend, R. H.; Gymer, R. W.; Holmes, A. B.; Burroughes, J. H.; Marks, R. N.; Taliani, C.; Bradley, D. D. C.; Dos Santos, D. A.; Bredas, J. L.; Logdlund, M.; Salaneck, W. R. *Nature* **1999**, *397*, 121−128.
(6) Bernius, M.; Inbasekaran, M.; O'Brien, J.; Wu, W. S. *Adv. Mater.* **2000**, *12*, 1737−1750.
(7) Mitschke, U.; Baüerle, P. *J. Mater. Chem.* **2000**, *10*, 1471−1507.
(8) Scherf, U.; List, E. J. W. *Adv. Mater.* **2002**, *14*, 477−489.
(9) Nalwa, H. S. *Handbook of Advanced Electronic and Photonic Materials and Devices*; Academic: San Diego, CA, 2001; Vol. 10.
(10) Adachi, C.; Tsutsui, T.; Saito, S. *Appl. Phys. Lett.* **1990**, *57*, 531−533.

10.1021/ja044455q CCC: $30.25

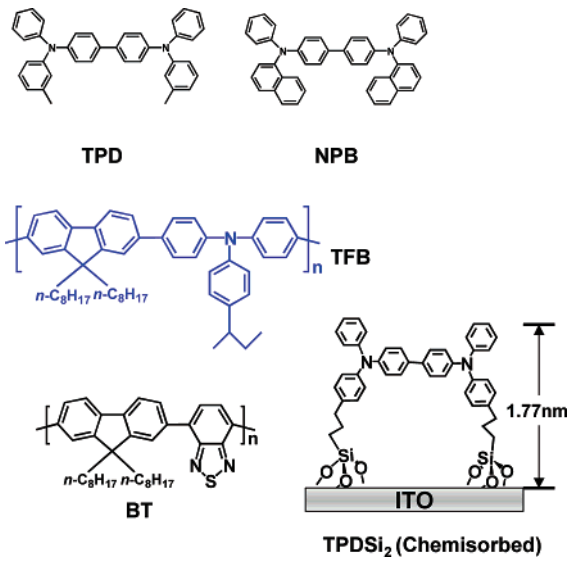

Figure 1. Chemical structures of small-molecule and polymer materials used to fabricate OLEDs and PLEDs.

small-molecule-based OLEDs fabricated via vacuum deposition. Typical small-molecule HTLs are triarylamine-based materials such as NPB or TPD (Figure 1), which are known to have appreciable hole-transporting and electron-blocking/exciton-blocking capacity because of their relatively high-lying lowest-unoccupied molecular orbital (LUMO) levels and large highest-occupied molecular orbital (HOMO)−LUMO gaps.

For polymer-based LEDs (PLEDs), while single-layer polymer devices have obvious attractions such as ease of fabrication, their performance is limited by inefficient hole injection from the ITO anode into the HOMO level of the EML polymer, as a result of, among other factors, the ITO work function (4.7 eV) and EML HOMO level (5.3−5.9 eV) mismatch.[12,13] Compared to its small-molecule counterparts, a multilayer PLED device is far more challenging to fabricate due to the risk of partially dissolving a previous layer while depositing the next in solution casting processes. Examples of conventional PLED HTLs are p-doped conductive polymers such as poly(3,4-ethylenedioxythiophene)-poly(styrenesulfonate) (PEDOT-PSS),[14−16] polyaniline-camphorsulfonic acid (PANI-CSA),[17,18] and polypyrrole-dodecylbenzene sulfonic acid (Ppy-BDSA).[19] In most cases, these HTL films are cured at high temperatures (∼200 °C) after spin-coating and thus rendered insoluble. These conventional HTLs have been shown to significantly enhance PLED anode hole injection[15] (by increasing the anode work function and smoothing energetic dicontinuities) and device performance.[20] However, these HTLs also have serious drawbacks such as corrosion of the ITO anode,[21,22] poor surface energy match with typical aromatic EMLs, and mediating the luminescence-degrading oxidative doping of polyfluorene EMLs.[23] Furthermore, the question still remains as to whether PEDOT-PSS has the magnitude of electron-blocking capacity required for a truly high-performance PLED HTL. In addition to these more conventional conductive polymer HTLs, there has also been intense research activity focused on photo- or thermally cross-linkable and *in situ* polymerized PLED HTLs.[24−28] Most of these cross-linkable HTLs require either high-temperature baking (150−200 °C)[24] or ultraviolet photochemical processing.[26] Moreover, many of these cross-linked films suffer from microcracking due to volume shrinkage[29] on cross-linking of the materials, which could lead to undesirable leakage currents in the PLED devices.

In previous work from this laboratory, we demonstrated that small-molecule OLED performance and durability can be significantly enhanced using triarylamine-based siloxane hole-transporting materials such as $TPDSi_2$ (Figure 1) as an anode hole injection/adhesion interlayer[11,30−36] ($TPDSi_2$ combines the hole-transporting capacity of TPD and the covalent-bonding capacity of organosilanol groups and can enhance OLED hole injection and device stability as a hole injection/adhesion interlayer). In this contribution, we present a full discussion of the application of organosiloxane cross-linking chemistry in developing a new family of cross-linkable HTLs for PLEDs. On the basis of these cross-linkable siloxane building blocks, we have devised three approaches to fabricating high-performance PLED HTLs: (1) $TPDSi_2$ self-assembled monolayers (SAMs), deposition of SAMs of $TPDSi_2$ onto the ITO anode as an ultrathin, covalently bonded HTL, which can completely alter the electronic and surface properties of ITO; (2) blended HTLs, spin-coating of a $TPDSi_2$ + TFB blend solutions onto the ITO anode, thereby forming heavily cross-linked, thermally robust, strongly adherent, and insoluble HTL interpenetrating coatings on ITO; (3) fabrication of double-layer HTLs with

(11) Huang, Q. L.; Cui, J.; Veinot, J. G. C.; Yan, H.; Marks, T. J. *Appl. Phys. Lett.* **2003**, *82*, 331−333.
(12) Parker, I. *J. Appl. Phys.* **1994**, *75*, 1656−1666.
(13) Brown, T. M.; Friend, R. H.; Millard, I. S.; Lacey, D. J.; Butler, T.; Burroughes, J. H.; Cacialli, F. *J. Appl. Phys.* **2003**, *93*, 6159−6172.
(14) Cao, Y.; Yu, G.; Zhang, C.; Menon, R.; Heeger, A. J. *Synth. Met.* **1997**, *87*, 171−174.
(15) Brown, T. M.; Kim, J. S.; Friend, R. H.; Cacialli, F.; Daik, R.; Feast, W. J. *Appl. Phys. Lett.* **1999**, *75*, 1679−1681.
(16) Groenendaal, B. L.; Jonas, F.; Freitag, D.; Pielartzik, H.; Reynolds, J. R. *Adv. Mater.* **2000**, *12*, 481−494.
(17) Yang, Y.; Heeger, A. H. *Appl. Phy. Lett.* **1994**, *64*, 1245−1247.
(18) Carter, S. A.; Angelopoulos, M.; Karg, S.; Brock, P. J.; Scott, J. C. *Appl. Phys. Lett.* **1997**, *70*, 2067−2069.
(19) Gao, J.; Heeger, A. J.; Lee, J. Y.; Kim, C. Y. *Synth. Met.* **1996**, *82*, 221−223.
(20) Elschner, A.; Bruder, F.; Heuer, H. W.; Jonas, F.; Karbach, A.; Kirchmeyer, S.; Thurm, S. *Synth. Met.* **2000**, *111*, 139−143.
(21) de Jong, M. P.; van IJzendoorn, L. J.; de Voigt, M. J. A. *Appl. Phys. Lett.* **2000**, *77*, 2255−2257.
(22) Wong, K. W.; Yip, H. L.; Luo, Y.; Wong, K. Y.; Lau, W. M.; Low, K. H.; Chow, H. F.; Gao, Z. Q.; Yeung, W. L.; Chang, C. C. *Appl. Phys. Lett.* **2002**, *80*, 2788−2790.
(23) Friend, R. H. *Mater. Res. Soc. Fall Meeting, Boston, MA, Dec.* **2002**, Lecture B4.6.
(24) Klarner, G.; Lee, J. I.; Lee, V. Y.; Chan, E.; Chen, J. P.; Nelson, A.; Markiewicz, D.; Siemens, R.; Scott, J. C.; Miller, R. D. *Chem. Mater.* **1999**, *11*, 1800−1805.
(25) Gong, X.; Moses, D.; Heeger, A. J.; Liu, S.; Jen, A. K. Y. *Appl. Phys. Lett.* **2003**, *83*, 183−185.
(26) Bacher, A.; Erdelen, C. H.; Paulus, W.; Ringsdorf, H.; Schmidt, H. W.; Schuhmacher, P. *Macromolecules* **1999**, *32*, 4551−4557.
(27) Müller, C. D.; Falcou, A.; Reckefuss, N.; Rojahn, M.; Wiederhirn, V.; Rudati, P.; Frohne, H.; Nuyken, O.; Becker, H.; Meerholz, K. *Nature* **2003**, *421*, 829−833.
(28) Liu, S.; Jiang, X. Z.; Ma, H.; Liu, M. S.; Jen, A. K. Y. *Macromolecules* **2000**, *33*, 3514−3517.
(29) Bailey, W. J.; Sun, R. L.; Katsuki, J.; Endo, T.; Iwama, H.; Tsusihma, R.; Saigou, K. *ACS Symp. Ser.* **1977**, *59*, 38−46.
(30) Li, W.; Wang, Q.; Cui, J.; Chou, H.; Marks, T. J.; Jabbour, G. E.; Shaheen, S. E.; Kippelen, B.; Pegyhambarian, N.; Dutta, P.; Richter, A. J.; Anderson, J.; Lee, P.; Armstrong, N. *Adv. Mater.* **1999**, *11*, 730.
(31) Cui, J.; Huang, Q.; Wang, Q.; Marks, T. J. *Langmuir* **2001**, *17*, 2051−2054.
(32) Cui, J.; Huang, Q.; Veinot, J. G. C.; Yan, H.; Marks, T. *Adv. Mater.* **2002**, *14*, 565−569.
(33) Cui, J.; Huang, Q.; Veinot, J. C. G.; Yan, H.; Wang, Q.; Hutchison, G. R.; Richter, A. G.; Evmenenko, G.; Dutta, P.; Marks, T. J. *Langmuir* **2002**, *18*, 9958−9970.
(34) Huang, Q. L.; Cui, J.; Yan, H.; Veinot, J. G. C.; Marks, T. J. *Appl. Phys. Lett.* **2002**, *81*, 3528−3530.
(35) Yan, H.; Huang, Q. L.; Cui, J.; Veinot, J. G. C.; Kern, M. M.; Marks, T. J. *Adv. Mater.* **2003**, *15*, 835−839.
(36) Yan, H.; Huang, Q.; Scott, B. J.; Marks, T. J. *Appl. Phys. Lett.* **2004**, *84*, 3873−3875.

PEDOT-PSS as the bottom layer and a $TPDSi_2$ + TFB interpenetrating network as the top one. These new HTLs are demonstrated to have very substantial hole-injection and electron-blocking capacities (the conventional PLED HTL, PEDOT-PSS, is shown to possess a significantly lesser electron-blocking capacity) and can enhance PLED performance to levels unattainable with conventional PLED HTLs. In addition, the present siloxane cross-linking process offers considerable convenience and flexibility and can be applied as a general strategy for fabricating high-performance PLED HTLs.

II. Experimental Section

Materials. Starting materials such as fluorene, *n*-butyllithium, and *n*-octyl bromide were purchased from Aldrich. Anhydrous toluene was purchased from Aldrich and passed through a Grubbs column system[37] to further remove O_2 and H_2O (the Grubbs column system consists of two 18-L stainless steel columns. The first column is packed with activated alumina, which removes polar impurities such as H_2O; the second one is packed with the copper catalyst, Q5, which removes trace O_2). Ethyl ether was dried over and distilled from Na/benzophenone. PEDOT-PSS in aqueous solution (Baytron P) was purchased from H. C. Starck, a Bayer company, and used without additional modification (Baytron P grade VP AI 4083 was used, which has a stated PEDOT/PSS ratio of 1:6 and a cast film resistivity of 1000 Ω·cm). All other reagents were used as received unless otherwise indicated. ITO-coated glass sheets (20 Ω/0, RMS roughness = 30−40 Å) were purchased from Colorado Concept Coating. Single-crystal Si (111) substrates for specular X-ray reflectivity measurements were purchased from Silicon Sense Inc.

General Physical Measurements. NMR analysis was performed with a Varian VXR-400 MHz NMR spectrometer using $CDCl_3$ as the solvent. Chemical shifts are referenced to the residual protonated solvent resonance. Elemental analysis was carried out at Midwest Microanalysis Lab (Indianopolis, IL). The structures of all organic materials are verified by NMR and elemental analysis. Thermogravimetric analysis (TGA) was carried out on an SDT 2960 simultaneous DTA-TGA instrument (TA Instruments) with a scan rate of 10 °C/min under N_2. Molecular weights of the polymers synthesized were measured vs polystyrene (PS) standards using a Waters room-temperature gel-permeation chromatography (GPC) system equipped with a Waters 2410 refractive index detector and a Waters 515 HPLC pump. Optical absorption spectroscopy of organic films was carried out with a Varian Cary 1E UV−visible instrument.

The morphologies of all thin films were evaluated by atomic force microscopy (AFM) using a Nanoscope III microscope with A and D scanners (Digital Instruments, Inc.). All images were recorded under ambient conditions in the contact mode with Si_3N_4 cantilevers having pyramidal tips with 70° cone angles and 20−50 nm radii of curvature. No attempt was made to account for tip convolution. The cantilever had a force constant of 0.12 N/m. The images were obtained using the height mode with a total force of 20−60 nN and a scan rate of ∼10 Hz. The same image was scanned at least three times to ensure the reproducibility as well as by scanning different area sizes (i.e., higher or lower magnifications) to verify image consistency. All the RMS surface-roughness values are reported over an area of 25 μm^2. Thicknesses of all organic thin films were measured using a Tencor P-10 surface profiler.

X-ray photoelectron spectroscopic (XPS) analyses were performed at Northwestern University with an Omicron ESCA probe, which was equipped with EA125 energy analyzer. Photoemission was stimulated by a monochromated Al Kα radiation (1486.6 eV) with the operating power of 300 W. A low-energy electron flood gun was employed for charge neutralization. Survey and high-resolution scans were collected using pass energies of 50 and 25 eV, respectively. Binding energies of spectra were referenced to the C 1s binding energy set at 284.8 eV.

The ionization potential (IP) and HOMO energies of $TPDSi_2$ SAM-modified ITO were determined by ultraviolet photoelectron spectroscopy (UPS) at the University of Arizona using a 21.2-eV He (I) source (Omicron H15-13) in a Kratos Axis-165 ultraphotoelectron spectrometer. The work functions of clean substrates were obtained by recording the difference in energy between the high kinetic energy onset and the low kinetic energy cutoff in these photoemission spectra. Samples were biased at +5 V to enhance the slope of the low kinetic energy cutoff region. Estimates of the high kinetic energy onset for photoionization were obtained by extrapolation of the high kinetic energy portion of the photoemission spectrum to the zero count baseline. For ITO samples with self-assembled films of the molecular modifiers, the HOMO and IP for the triarylamine cores of these modifiers were obtained from the UPS data, correcting for shifts in a vacuum level relative to the clean ITO substrate.[38] HOMO values were estimated from the median energy of the clearly defined photoemission peak, while IP values were estimated from the extrapolation of the high kinetic energy edge of that peak to zero intensity. Both values reported were corrected for apparent shifts in a vacuum level. There is a difference of ca. 0.8 eV between the median HOMO energy and the IP owing to the width of the photoemission peak in these samples, which has been observed in previous UPS studies of such triarylamines.[39]

The ionization potential (IP) and work function of $TPDSi_2$ SAM-modified ITO were determined by UPS at the University of Arizona using the 21.2-eV He (I) source (Omicron H15-13) of a Kratos Axis-165 ultraphotoelectron spectrometer. Work functions of the clean substrates were obtained by recording the difference in energy between the high kinetic energy onset and the low kinetic energy cutoff for photoionization. Samples were biased at ±5 V to enhance the slope of the low kinetic energy cutoff region. Estimates of the high kinetic energy onset for photoionization were obtained by extrapolation of the high kinetic energy portion of the photoemission spectrum to the zero count baseline. For ITO samples with self-assembled films of the molecular modifiers, HOMO and IP values for the triarylamine cores of these modifiers were obtained from the UPS data, correcting for shifts in a vacuum level relative to the clean ITO substrate.[38] HOMO values were estimated from the median energy of the clearly defined photoionization peak, while IP values were estimated from the extrapolation of the high kinetic energy edge of that peak to zero intensity. Both values reported were corrected for apparent shifts in a vacuum level.

Synthesis of Poly(9,9-dioctylfluorene-*co*-N-(4-(3-methylpropyl))-diphenylamine) (TFB). TFB was synthesized from 2,7-bis(4,4,5,5-tetramethyl-1,3,2-dioxaborolan-2-yl)-9,9-dioctylfluorene and 4-(3-methylpropyl)-*N*,*N*-bis(4-bromophenyl)aniline using conventional Suzuki coupling methodology[40] and procedures similar to those discribed in the patent literature.[41] The reagents 2,7-bis(4,4,5,5-tetramethyl-1,3,2-dioxaborolan-2-yl)-9,9-dioctylfluorene and 4-(3-methylpropyl)-*N*,*N*-bis-(4-bromophenyl)aniline were synthesized using procedures similar to those as described in either in patent[41] or journal literature,[43] respectively. Experimental details are as follows.

To a mixture of purified 4-(3-methylpropyl)-*N*,*N*-bis(4-bromophenyl)aniline (0.459 g, 1.0 mmol) and 2,7-bis(4,4,5,5-tetramethyl-1,3,2-dioxaborolan-2-yl)-9,9-dioctylfluorene (0.642 g, 1.0 mmol) in 10 mL

(37) Pangborn, A. B.; Giardello, M. A.; Grubbs, R. H.; Rosen, R. K.; Timmers, F. J. *Organometallics* **1996**, *15*, 1518−1520.
(38) Alloway, D. M.; Hofmann, M.; Smith, D. L.; Gruhn, N. E.; Graham, A. L.; Colorado, R.; Wysocki, V. H.; Lee, T. R.; Lee, P. A.; Armstrong, N. R. *J. Phys. Chem. B* **2003**, *107*, 11690−11699.
(39) Schmidt, A.; Anderson, M. L.; Armstrong, N. R. *J. Appl. Phys.* **1995**, *78*, 5619−5625.
(40) Miyaura, N.; Suzuki, A. *Chem. Rev.* **1995**, *95*, 2457−2483.
(41) Towns, C. R.; O'Dell, R. *PCT Int. Appl.* 2000.
(42) Ranger, M.; Rondeau, D.; Leclerc, M. *Macromolecules* **1997**, *30*, 7686−7691.
(43) Wenseleers, W.; Stellacci, F.; Meyer-Friedrichsen, T.; Mangel, T.; Bauer, C. A.; Pond, S. J. K.; Marder, S. R.; Perry, J. W. *J. Phys. Chem. B* **2002**, *106*, 6853−6863.

of oxygen-free toluene under nitrogen was added 0.10 g (0.25 mmol) of the phase-transfer catalyst "Aliquat 336" and 6 mL of 2 M aqueous Na_2CO_3 solution (the Na_2CO_3 solution was purged with N_2 for 10 min before being added to the reaction); the mixture was then stirred under nitrogen for 20 min, followed by the addition of 3 mg (4 μmol) of tetrakis(triphenylphosphine)palladium(0) as the catalyst. The reaction was vigorously stirred at ~120 °C for 4−6 h to yield a highly viscous mixture; to reduce viscosity and maintain vigorous stirring, 5−10 mL of toluene was then added. The reaction mixture was maintained under the same conditions for 10 h, after which 0.10 mL (0.80 mmol) of phenylethylene boronate was added. After another 10 h of reaction time, 0.30 mL (2.2 mmol) of bromobenzene was added as an end-capping agent. The reaction mixture was poured into 400 mL of methanol after an additional 5 h, and the precipitated polymeric product was collected to afford 0.70 g of pale yellow polymer. The polymer was then carefully purified by repetitive dissolution in toluene and precipitation with methanol to remove ionic impurities and catalyst residues. The number and weight average molecular weights (M_n and M_w) of the TFB obtained by this procedure were determined to be 31 000 and 88 000 (polydispersity = 2.88), respectively, by GPC using THF as the eluent and PS standards. ^{1}H NMR (400 MHz, $CDCl_3$): δ(ppm) 7.76 (d, J = 6.8 Hz, 2H), 7.62 (s, 2H), 7.59 (d, J = 9.2 Hz, 2H), 7.26 (d, J = 6.0 Hz, 4H), 7.02−6.99 (m, 8H), 2.64−2.60 (m, 1H), 2.05 (m, 4H), 1.66−1.60 (m, 2H), 1.28 (t, J = 6.4 Hz, 3H), 1.20−1.00 (m, 20H), 0.89 (t, J = 6.0 Hz, 3H), 0.81 (t, J = 5.2 Hz, 6H), 0.74 (m, 4H). Anal. Calcd. for $C_{51}H_{61}N$: C, 89.08; H, 8.88; N, 2.04. Found: C, 89.38; H, 8.44; N, 2.18.

Synthesis of Poly(9,9-dioctylfluorene-*co*-benzothiadiazole) (BT). BT was synthesized from 2,7-bis(4,4,5,5-tetramethyl-1,3,2-dioxaborolan-2-yl)-9,9-dioctylfluorene and 4,7-dibromo-2,1,3-benzothiadiazole using conventional Suzuki coupling methodology[40] and procedures similar to those described in a patent reference.[41] The reagent 4,7-dibromo-2,1,3-benzothiadiazole was synthesized using a procedure similar to that described in the literature.[44] Experimental details are described as follows.

Under inert atmosphere, a 50-mL reaction flask was charged with 0.15 g (0.51 mmol) of purified 4,7-dibromo-2,1,3-benzothiadiazole and 3 mL of oxygen-free THF. Next, the 4,7-dibromo-2,1,3-benzothiadiazole mixture was brought to ~60 °C with stirring, at which point the benzothiadiazole dissolved. Bis(tetraethylammonium) carbonate (1.0 g, 3.0 mol) in 2 mL of deionized water was purged with N_2 gas for 10 min and then added to the reaction flask, and the mixture was stirred under N_2 for 10 min. Next, 2,7-bis(4,4,5,5-tetramethyl-1,3,2-dioxaborolan-2-yl)-9,9-dioctylfluorene (0.34 g, 0.52 mmol) was dissolved in 3 mL of toluene, purged with N_2 gas for 10 min, and added to the reaction flask. The reaction mixture was stirred under N_2 for 20 min before addition of 3 mg (4 μmol) of the catalyst $(Ph_3P)_4Pd$. The reaction mixture was vigorously stirred and refluxed at 90 °C for 18 h, during which time the reaction mixture became highly viscous. Bromobenzene (0.10 mL, 0.70 mmol) was then added, and after 10 h, phenylethylene boronate (0.30 mL, 2.4 mmol) was added as an end-capping reagent. The reaction mixture was poured into 300 mL of methanol after 5 h, and the precipitated polymer was collected to afford 0.3 g of yellow fibrous product. The polymer was then carefully purified by repetitive dissolution in toluene and precipitation with methanol to remove ionic impurities and catalyst residues. The M_n and M_w values of the BT produced in this procedure were determined to be 143 000 and 269 000 (polydispersity = 1.88), respectively, by GPC using THF as the eluent and PS standards. ^{1}H NMR (400 MHz, $CDCl_3$): δ(ppm), 8.10−7.97 (m, 8H), 2.18−2.10 (m, 4H), 1.25−0.96 (m, 24H), 0.81 (t, J = 6.4 Hz, 6H). Anal. Calcd. for $C_{35}H_{42}N_2S$: C, 80.46; H, 8.05; N, 5.36; S, 6.13. Found: C, 80.22; H, 8.16; N, 5.32; S, 6.30.

Fabrication Procedure for $TPDSi_2$ SAMs. Clean ITO substrates were first treated with an O_2 plasma for 3 min and then transferred to a dry, clean Schlenk flask. Following strict Schlenk protocol, the Schlenk flask was further dried using a flame or a heatgun, followed by addition of a 1.0 mM dry toluene solution of $TPDSi_2$ to the Schlenk flask by syringe. The ITO substrates were immersed in the $TPDSi_2$ solution at ~95 °C for 40 min, followed by rinsing and sonication with anhydrous toluene 3 times. The substrates were next immersed in a water/acetone mixture (1:100) with sonication for 5 min and then transferred to a 120 °C oven for 30 min.

Specular X-ray Reflectivity Measurements. Specular X-ray reflectivity experiments on coated single-crystal Si (111) substrates were performed at the Naval Research Laboratory X23B beamline at the National Synchrotron Light Source. Details of this measurement procedure and subsequent data analysis are described elsewhere.[31,33,45,46]

Deposition of Conventional PEDOT-PSS HTLs. For the deposition of PEDOT-PSS, ITO substrates were first washed using the standard organic solvent/ sonication procedures described above and then cleaned with an oxygen plasma treatment, immediately followed by spin-coating of the commercial PEDOT-PSS solution onto the ITO at ~3000 rpm. The resulting films were then cured on a hotplate in air at ~150−200 °C for 10 minn and stored in an inert atmosphere glovebox prior to $TPDSi_2$ + TFB blend or EML deposition.

Deposition of Spin-Coated $TPDSi_2$ + TFB Blend Films. For the deposition of $TPDSi_2$ + TFB blend coatings, ITO substrates were cleaned using the standard organic solvent/sonication procedure; however, the usual oxygen plasma treatment was found to be unnecessary. $TPDSi_2$ and TFB solutions (concentrations of each were ~2.5 mg/mL) in anhydrous toluene were first prepared in an inert atmosphere glovebox (O_2 and moisture levels < 1 ppm) and then blended (mass ratio of $TPDSi_2$:TFB = 1:1). This blend solution was transferred from the glovebox using a sealed syringe and then spin-coated onto the clean ITO substrates at ~3000 rpm (film thickness of $TPDSi_2$ + TFB ~15 nm). The resulting film was dried at ~90 °C in a vacuum oven (15 Torr) for 0.5 h and stored in the glovebox before EML spin-coating.

Solubility Test of $TPDSi_2$ + TFB Blend Films. The optical absorption spectrum of a $TPDSi_2$ + TFB blend (1:1 mass ratio) film was recorded using a Varian Cary 1E UV−vis spectrophotometer. Xylenes (~1 mL, the solvent for EML spin-coating) were then spin-coated onto a $TPDSi_2$ + TFB blend film prepared by the aforementioned procedure, followed by drying in a vacuum oven at 90 °C for 5 min. The optical absorption spectra of the same $TPDSi_2$ + TFB blend film before and after xylene spin-coating were measured vs the same blank substrate, using the same spectrometer and the same instrumental setup, and compared.

PLED Device Fabrication. Two series of PLED devices were fabricated using $TPDSi_2$ SAMs, the blend HTLs, and the double-layer HTLs. PLEDs based on PEDOT-PSS were also fabricated as controls. The first series using TFB + BT (1:4) blend as the EML will be referred to as the (TFB + BT)-based series; the device structure is a ITO/HTL/TFB + BT (1:4) blend (70 nm)/Ca (10 nm)/Al (100 nm). The second device series using BT as the EML will be referred to as the BT-based series; the device structure is ITO/HTL/BT (70 nm)/Ca (10 nm)/Al (100 nm). The structures investigated are summarized in Figure 2. EMLs were spin-coated onto HTL-coated substrates from xylene solutions to afford an EML thickness of ~70 nm as measured by step profilometry. The resultant films were then dried in a vacuum oven at ~90 °C overnight and then taken into the glovebox. Inside an inert-atmosphere glovebox, Ca was thermally evaporated onto the EML under a vacuum of $<10^{-6}$ Torr, using a shadow mask to define the electrode area as 10 mm^2 and followed by Al deposition as a protective layer. The resulting PLED devices were characterized inside a sealed aluminum sample container under a dry nitrogen atmosphere using a computer-controlled

(44) Pilgram, K.; Zupan, M.; Skiles, R. *J. Heterocycl. Chem.* **1970**, *7*, 629−633.
(45) Roscoe, S. B.; Kakkar, A. K.; Marks, T. J.; Malik, A.; Durbin, M. K.; Lin, W. P.; Wong, G. K.; Dutta, P. *Langmuir* **1996**, *12*, 4218−4223.
(46) Malik, A.; Lin, W.; Durbin, M. K.; Marks, T. J.; Dutta, P. *J. Chem. Phys.* **1997**, *107*, 645−652.

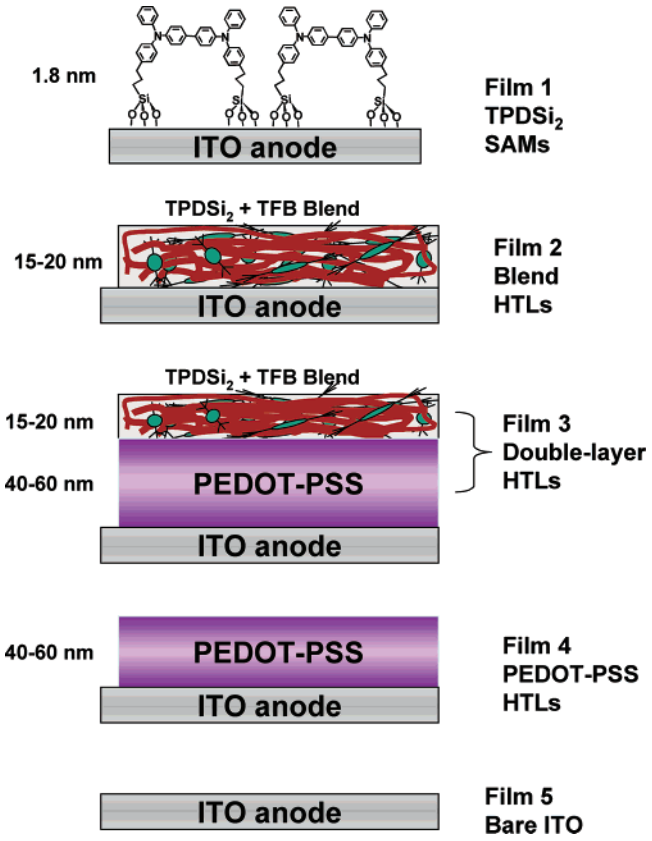

Figure 2. Anode/HTL structures used in the present study.

Keithley 2400 source meter and an IL 1700 Research Radiometer equipped with a calibrated silicon photodetector.[31,47]

Hole-Only Device Fabrication. A series of hole-only devices of structure ITO/ HTL/TFB (75 nm)/Au (14 nm)/Al (120 nm) were also fabricated using the deposition procedures described. The current density−voltage (I−V) responses of the present hole-only devices were characterized on a probe station using the same computer-controlled Keithley 2400 source meter.

III. Results

In this section, we first discuss surface characterization results for $TPDSi_2$ SAMs and $TPDSi_2$ + TFB blend films on ITO or on PEDOT-PSS-coated ITO substrates. Device response characteristics of PLEDs based on the $TPDSi_2$ SAM, the $TPDSi_2$ + TFB blend HTL, and the double-layer HTL (Figure 2) are then compared using EMLs with predominant electron transport or balanced hole and electron transports. PLED devices using conventional PEDOT-PSS HTLs were also fabricated and examined as controls. Finally, the hole-injection capacities of various HTLs are evaluated and compared using hole-only devices.[12]

Characterization of $TPDSi_2$ SAMs. UPS characterization of the $TPDSi_2$ SAM-modified ITO showed that the IP for the covalently attached triarylamine is ca. 5.2 eV (Figure 3) and that the HOMO median energy is ca. 6.1 eV, after correction for shifts in a vacuum level introduced by this molecular modifier.[38,48] The difference in HOMO and IP energies arises from the rather broad photoemission bands for these triarylamines.[39] The vacuum level shift/interface dipole creation upon $TPDSi_2$ SAM modification is determined to be ∼+0.1 eV, which should, in principle, reduce the intrinsic hole injection barrier and hence enhance hole injection. In contrast, the work function of bare ITO is found to be 4.5 eV, in general agreement with literature values.[49,50]

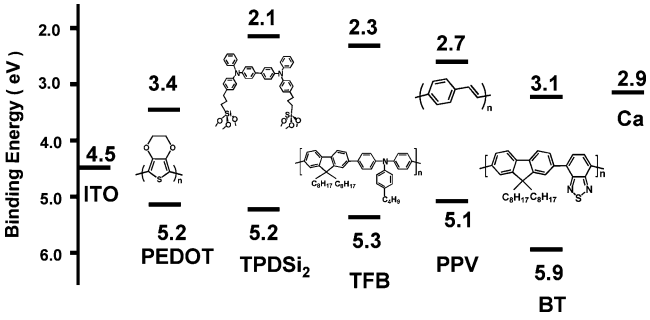

Figure 3. Energy diagram of PLED components. Energy levels of small molecule materials, NPB, TPD, and Alq and polymer materials BT, TFB, and PEDOT are commonly accepted values cited from the literature.[15,34,57,61,62] The energy levels for $TPDSi_2$ are estimated by UPS and optical band-gap measurements.

X-ray reflectivity (XRR) measurements on the $TPDSi_2$ SAM deposited on single-crystal Si (111) substrates yield a thickness of 1.77 nm (close to the value of ∼1.44 nm estimated by the approximate AM1-level calculations, Figure 1), suggesting that most $TPDSi_2$ molecules are chemisorbed on the substrate in an approximately "upright" orientation (Figure 1).

The advancing aqueous contact angle of the $TPDSi_2$ SAM-modified ITO is 80°, while the relevant angles for clean ITO, ITO/PEDOT-PSS, and TFB surfaces are 0−20, 30, and 90°, respectively. It is generally accepted [31,32,51,52] that interfacial affinity plays an important role in the response properties of organic LEDs. The surface energy mismatch between hydrophilic ITO and a hydrophobic polymer is likely to cause poor physical-electronic contact at the ITO/polymer interface and hence inefficient anode hole injection as well as thermal instability. Modification of ITO anodes with $TPDSi_2$ SAMs reduces the surface energy mismatch at the ITO/polymer interface and is likely to facilitate PLED anode hole injection, since previous work indicated that it enhances hole injection into small-molecule hole transport structures.[31−33]

Characterization of $TPDSi_2$ + TFB Blends on ITO. The optical absorption spectra of $TPDSi_2$ + TFB (1:1 mass ratio) blend films on ITO substrates were recorded before and after rinsing with xylene. Figure 4A shows that after spin-coating xylene (the solvent for deposition of the EML) onto the cross-linked $TPDSi_2$ + TFB HTL, the optical absorption of the $TPDSi_2$ + TFB film remains essentially unchanged, indicating insolubility of the cured $TPDSi_2$ + TFB blend under the conditions incurred on spin-coating the EML. However, without the cross-linkable $TPDSi_2$ in the blend, the TFB-only HTL is readily dissolved by xylene spin-coating (Figure 4B).

The composition of the $TPDSi_2$ + TFB blend films was also investigated by XPS. A significant issue for conventional PLED HTLs such as PEDOT-PSS is that its solutions have a pH value

(47) Li, W.; Wang, Q.; Cui, J.; Chou, H.; Marks, T. J.; Jabbour, G. E.; Shaheen, S. E.; Kippelen, B.; Pegyhambarian, N.; Dutta, P.; Richter, A. J.; Anderson, J.; Lee, P.; Armstrong, N. *Adv. Mater.* **1999**, *11*, 730−734.
(48) Carter, C.; Graham, A.; Armstrong, N.; Yan, H.; Marks, T. J., unpublished results, 2004.
(49) Osada, T.; Kugler, T.; Broms, P.; Salaneck, W. R. *Synth. Met.* **1998**, *96*, 77−80.
(50) Kim, J. S.; Granstrom, M.; Friend, R. H.; Johansson, N.; Salaneck, W. R.; Daik, R.; Feast, W. J.; Cacialli, F. *J. Appl. Phys.* **1998**, *84*, 6859−6870.
(51) Yu, W.; Pei, J.; Cao, Y.; Huang, W. *J. Appl. Phys.* **2001**, *89*, 2343.
(52) Choi, B.; Rhee, J.; Lee, H. H. *Appl. Phys. Lett.* **2001**, *79*, 2109−2111.

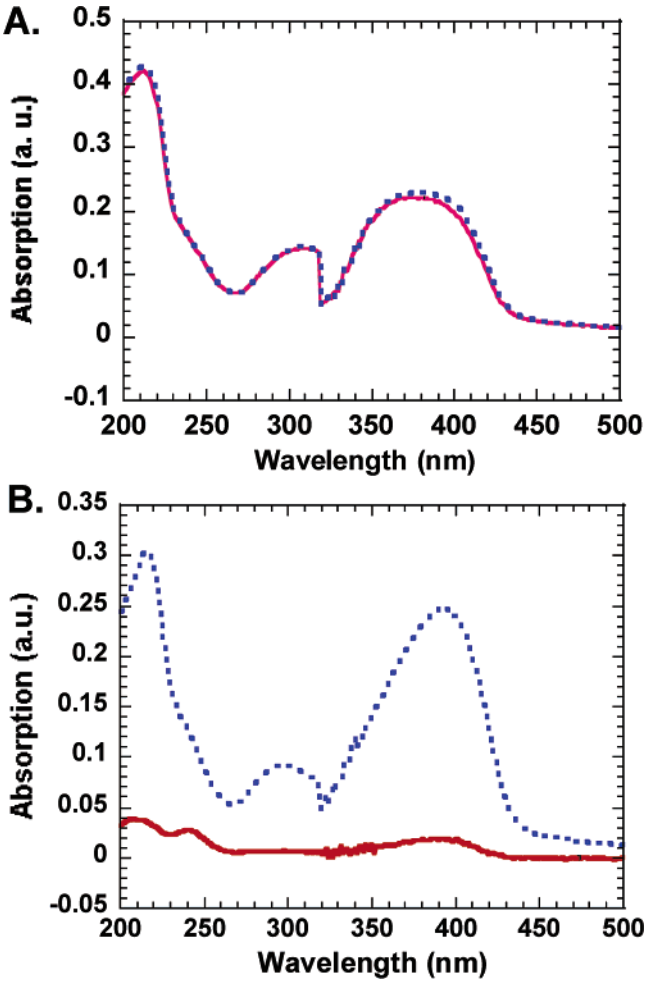

Figure 4. Optical absorption spectra of: (A) $TPDSi_2$ + TFB HTL; (B) TFB-only film, before and after the xylene solubility test. Dotted line, before rinsing; solid line, after rinsing.

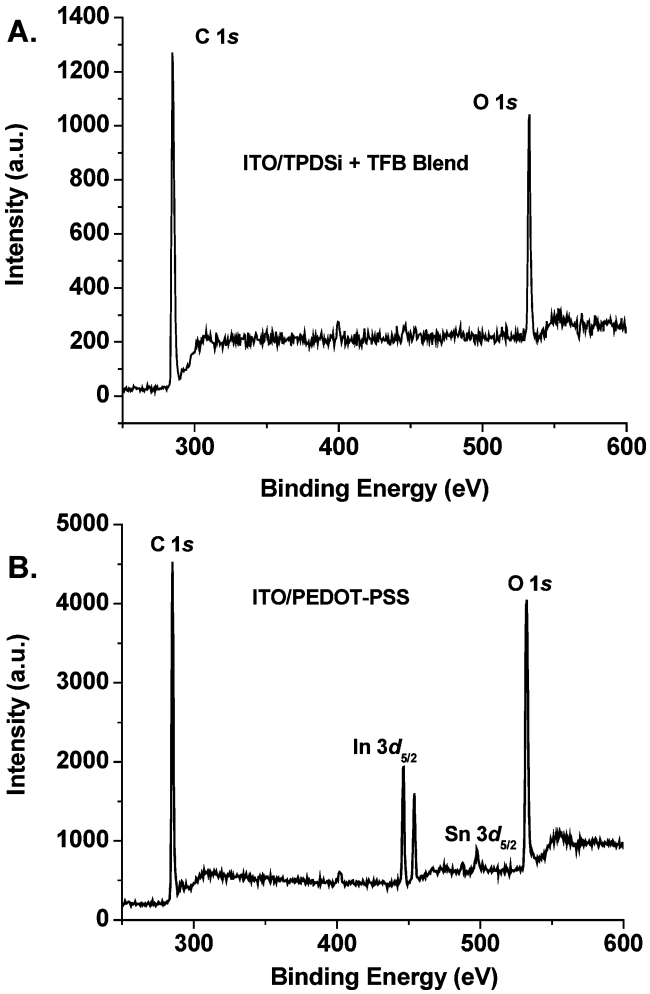

Figure 5. XPS spectra of: (A) ITO/$TPDSi_2$ + TFB blend; (B) ITO/PEDOT-PSS using 1486.6 eV monochromated Al Kα radiation with an operating power of 300 W.

of ∼1,[21,22] and ITO is known to be sensitive to corrosion by aqueous acids.[21,22] Indeed, PEDOT-PSS has been shown to undergo reaction with ITO and to introduce indium contamination into the HTL and EML structures.[21,22] In the present work, we employed XPS to study the film compositions of PEDOT-PSS and the $TPDSi_2$ + TFB blend on ITO substrates after casting. The substrates were then heated in an oven (120 °C) under air for 1 week. The final indium composition in PEDOT-PSS is determined to be ∼1.5%, while that in the $TPDSi_2$ + TFB film is below the instrumental detection limit (<0.05 atom % for indium). The XPS spectra of PEDOT-PSS and $TPDSi_2$ + TFB blend films on ITO are compared in Figure 5.

A similar solubility test verifies that the $TPDSi_2$ + TFB blend on the PEDOT-PSS-coated ITO is also insoluble under the xylene spin-coating procedure. Furthermore, XPS measurements verify that there is negligible indium contamination in the $TPDSi_2$ + TFB blend film on PEDOT-PSS-coated ITO after heating under air at 120 °C for one week.

Surface Morphology Study. The surface morphologies of $TPDSi_2$ SAMs (film 1), the $TPDSi_2$ + TFB blend HTL (film 2), the double-layer HTL (film 3), the PEDOT-PSS HTL (film 4), and bare ITO substrates (film 5) were studied by contact-mode AFM. The RMS roughness of the present ITO substrates was determined by AFM to be 3.0−4.0 nm. The RMS roughnesses of films 1, 2, 3, and 4 were determined to be 3.9, 1.7, 1.0, and 1.1 nm, respectively, while the film thicknesses of films 1, 2, 3, and 4 were determined by surface profilometry to be 1.8, 15, 60, and 45 nm respectively. Thus, it can be clearly seen that the $TPDSi_2$ SAM provides conformal coverage of the $TPDSi_2$ molecules on the ITO but has no significant planarization effects. In contrast, the blend HTL achieves considerable planarization on ITO, while the planarizations imparted by the double-layer HTL and the PEDOT-PSS HTL are greater still.

Response Comparison of PLED Devices based on Films 1, 2, 3, and 4 with the TFB + BT Blend as the EML. The response characteristics of BT-based PLEDs fabricated on films 1, 2, 3, and 4 are compared in parts A and B of Figure 6 for luminance−voltage (L−V) and current efficiency−voltage (CE−V) properties, respectively. The double-layer HTL-based device (ITO/PEDOT-PSS/$TPDSi_2$ + TFB blend) exhibits the most impressive performance: it turns on at ∼2.3 V and reaches a maximum current efficiency of ∼17 cd/A at 5−6 V. The double-layer HTL and the blend HTL-based devices can withstand current densities as high as 2 A/cm^2, and at this current density level, the device exhibits maximum luminance of ∼140,000 cd/m^2 and still exhibits current efficiencies as high as 13 cd/A. Compared to the control device with PEDOT-PSS as the HTL, the present double-layer HTL and blend HTL-based devices exhibit 70 and 40% greater current efficiencies, respectively, and 2-fold greater maximum light output.

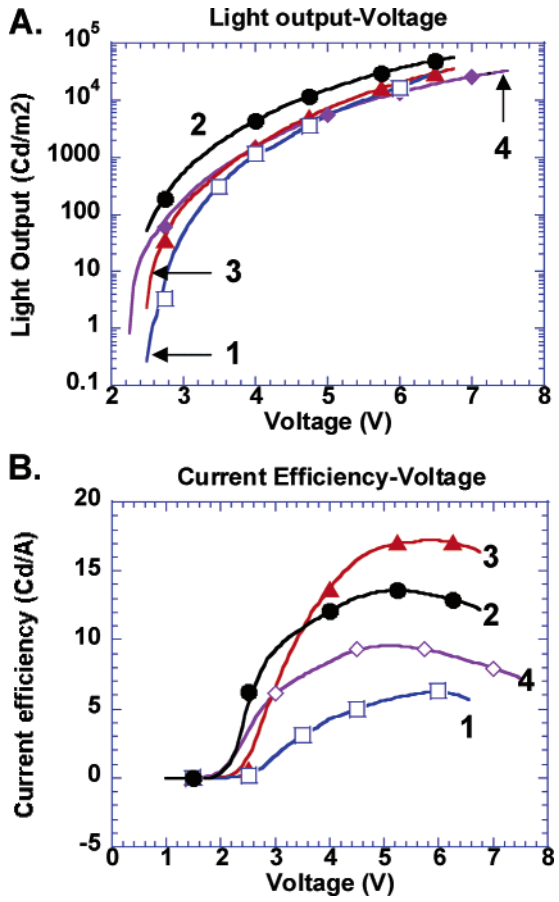

Figure 6. (A) Light output, B. CE−V characteristics as a function of operating voltage for PLED devices having the structure ITO/HTL/TFB + BT blend/Ca/Al. The HTLs compared are: (1, 0) $TPDSi_2$ SAM; (2, b) the blend HTL; (3, 2) double-layer HTL; (4,]) PEDOT-PSS. Lines through the data points are drawn as a guide to the eye.

Hole Injection Capacity Comparison of Structures 1, 2, 3, 4, and 5 as Assessed by Hole-Only Devices. The current density vs electric field characteristics of TFB-based hole-only devices fabricated with films 1, 2, 3, 4, and 5 are compared in Figure 7. The hole-injection fluence of devices based on structures 1, 2, 3, and 4 are 50−200-fold greater than that of a bare ITO-based device. These data show that $TPDSi_2$ SAM, the blend HTL, and the double-layer HTL all provide ∼100-fold greater hole injection compared to bare ITO anodes and comparable hole injection compared to the PEDOT-PSS HTL.

Response Comparison of Devices based on Structures 1, 2, 3, 4, and 5 with BT as the EML. As implied by its HOMO and LUMO energies (Figure 3), BT is a highly electron-dominated emissive polymer. Therefore, in a BT/Ca-based PLED device, there is a substantial cathode-originating electron current reaching the HTL/ EML interface, and a BT/Ca-based PLED device is therefore a convenient model to assess the electron-blocking properties of an HTL at the HTL/EML interface. The response characteristics of BT-based devices using structures 1, 2, 3, 4, and 5 are compared in parts A, B, and C of Figure 8 for L−V, CE−V, and current I−V responses, respectively. The turn-on voltages of the present BT-based devices fabricated with films 1, 2, 3, 4, and 5 are 3.1, 3.5, 4.3, 5.5, and 10 V, respectively (turn-on voltage is defined as the voltage required for a device to reach a luminance of ∼1 cd/m^2). The most efficient blend HTL-based device achieves a

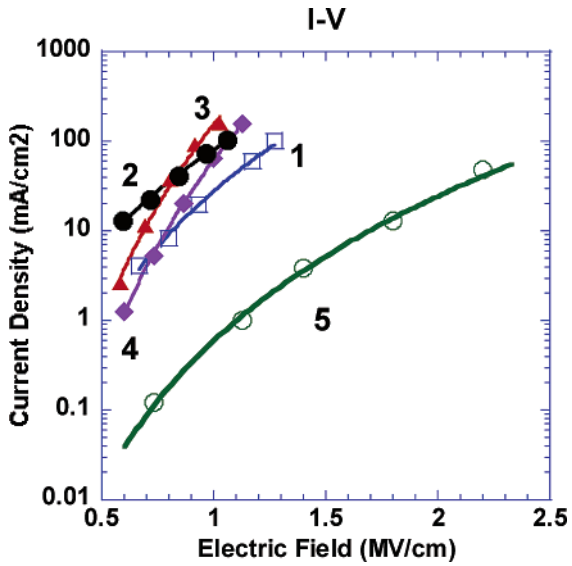

Figure 7. Current density vs electric field response for hole-only devices having the structure ITO/HTL/TFB/Au/Al. The HTLs compared are: (1, 0) $TPDSi_2$ SAM; (2, b) the blend HTL; (3, 2) the double layer HTL; (4,]) PEDOT-PSS; (5, O) bare ITO. Lines through the data points are drawn as a guide to the eye.

current efficiency of 10−11 cd/A in the 6−8 V range, while the most efficient double-layer HTL-based device exhibits a current efficiency of 15−17 cd/A in the 6−8 V range. These values of maximum current efficiency are ∼1000-fold greater than those of the bare ITO-based device. Furthermore, compared to the device with PEDOT-PSS alone as the HTL, the present blend HTL and double-layer HTL-based devices achieve ∼10-fold greater current efficiency, clearly a result of effective electron-blocking at the HTL/EML interface.

IV. Discussion

Increased Hole Injection upon Modification of ITO with an Ultrathin $TPDSi_2$ SAM or the $TPDSi_2$ + TFB Blend HTL. As shown in Figure 7, the $TPDSi_2$ SAM-modified ITO anode provides ∼2 orders of magnitude greater hole injection from the anode into a PLED device compared to one having a bare ITO anode. This behavior can be rationalized by the following effects.

Modification of Surface Properties. As discussed earlier, modification of ITO anodes with a $TPDSi_2$ SAM completely changes the ITO surface hydrophilicity, and minimizes the surface energy mismatch between hydrophilic ITO and a hydrophobic polymer. It has been widely recognized that interfacial energetics play an important role in the response characteristics of organic LEDs.[31,32,51−53] The improved interfacial affinity between the modified ITO and the active polymer is likely the major reason for the enhanced hole injection by $TPDSi_2$ SAMs. It is also possible that this surface functionalization effect is further enhanced by the favorable interface dipole/vacuum level shift detected in the UPS studies.

Chemical Bonding between $TPDSi_2$ SAMs and ITO Anodes. It is also important to note that there is only physical contact between a typical light-emitting polymer and a bare ITO anode; however, for a SAM-modified PLED device, $TPDSi_2$ SAMs are chemically bonded to the ITO anode, which is likely to

(53) Huang, Q. L.; Evmenenko, G.; Dutta, P.; Marks, T. J. *J. Am. Chem. Soc.* **2003**, *125*, 14704−14705.

Table 1. Comparison of Maximum Current Efficiencies and Turn-On Voltages of PLED Devices Having the Structure ITO/HTL/TFB + BT Blend/Ca/Al[a]

	$TPDSi_2$ + TFB	C_6Si_2 + TFB	$TPDSi_2$ + PS
maximum current efficiency (cd/A)	13.5	9.0	8.5
turn-on voltage (V)	2.0	3.0	2.5

[a] The HTLs compared are: 1, $TPDSi_2$ + TFB blend; 2, C_6Si_2 + TFB blend; 3, $TPDSi_2$ + PS blend.

afford closer, more thermally robust contact of the $TPDSi_2$ SAM hole transporting units to the ITO anode and hence more efficient hole injection.

The next question that arises is why the $TPDSi_2$ + TFB blend HTL so effectively enhances hole injection. For example, hole-only device 2 (ITO/$TPDSi_2$ + TFB/TFB/Au/Al) exhibits 200-fold greater hole-injection fluence than hole-only device 5 (ITO/TFB/Au/Al). At the $TPDSi_2$ + TFB/TFB interface in device 2, hole transport can propagate through the same TFB structure, with near-perfect HOMO level alignment. Therefore, the difference in hole-injection characteristics between devices 2 and 5 reasonably originates from the very different nature of the ITO/TFB and ITO/$TPDSi_2$ + TFB interfaces. For device 5, there is no covalent bonding between the ITO surface and the TFB layer. Thus, the surface energy mismatch between ITO and TFB and the 0.8-eV intrinsic hole injection barrier from ITO to TFB are likely causes for the poor hole-injection performance. For device 2, however, $TPDSi_2$ is covalently bonded to the ITO surface, which brings the $TPDSi_2$ hole-transporting units in very close contact (<1 nm) with the ITO surface. Furthermore, the fact that the TFB polymer chains are immobilized within the cross-linked $TPDSi_2$ matrix may also force some fraction of hole-transporting TFB chains into close contact with the ITO anode, and as a consequence, hole injection from ITO into the HTL is facilitated. (If TPD were used to replace $TPDSi_2$ in the $TPDSi_2$ + TFB blend, the blend would be easily dissolved by the spin-coating of the next layer.) Our results clearly show that chemical bonding between the HTL and the ITO anode plays an essential role in achieving efficient anode hole injection.

Both $TPDSi_2$ and TFB Contribute to the Hole-Transporting Capacity of the $TPDSi_2$ + TFB Blend. The next question arises as to how $TPDSi_2$ and TFB contribute to the hole transporting capacity of the $TPDSi_2$ + TFB blend. To answer this question, we fabricated PLED devices with the structure ITO/HTL/TFB + BT (1:4) blend (70 nm)/Ca (10 nm)/Al (100 nm) with the HTL being: (1) $TPDSi_2$ + TFB blend; (2) $TPDSi_2$ + PS blend; or (3) 1,6-bis(trichlorosilyl)hexane (C_6Si_2) + TFB blend. PS and C_6Si_2 are electric insulating materials; therefore, HTL 2 or 3 consists of only one hole-transporting component, $TPDSi_2$ or TFB, and the contribution of $TPDSi_2$ or TFB to the hole transporting capacity of the $TPDSi_2$ + TFB blend can be separately evaluated. The L−V and CE−V responses of the device based on HTL 1 was shown in Figure 6: maximum current efficiency, is ∼13.5 cd/A; turn-on voltage, ∼2.0 V. The key performance characteristics of the present PLED devices based on HTLs 1, 2, and 3 are compared in Table 1. PLED devices based on HTLs 2 and 3 exhibit maximum current efficiencies of ∼8.5−9.0 cd/A and turn-on voltages of ∼2.5−3.0 V. This result suggests that both $TPDSi_2$ and TFB significantly contribute to the hole-transporting properties of the $TPDSi_2$ + TFB blend.

Electron Blocking Capacity of PEDOT-PSS vs the $TPDSi_2$ + TFB Blend. The functions of an effective HTL are not only to maximize hole injection from the anode but also to block electron overflow from, and to confine excitons within, the EML. However, it is not clear from a number of standpoints whether PEDOT-PSS has sufficient electron-blocking capacity for a truly high-performance PLED HTL. For example, PEDOT-PSS has much greater conductivity than, and a distinctively different core structure from, conventional electron-blocking triarylamine small-molecule HTLs and may have significantly different levels of electron-blocking properties. In the recent work by Morgado et al.,[54] the maximum current efficiency of a polyfluorene-based PLED was nearly doubled by inserting a poly(phenylenevinylene) (PPV) electron confinement layer between the PEDOT-PSS HTL and the EML. This result suggests that PEDOT-PSS HTLs do not possess as great of an electron-blocking capacity as PPV.

The present $TPDSi_2$ + TFB blend has a similar triarylamine core structure to those of classic HTL/electron-blockers such as NPB and TPD and is likely to have comparable electron-blocking properties. For these reasons, it was of interest to determine whether the $TPDSi_2$ + TFB blend has greater electron-blocking capacity than does PEDOT-PSS and also to determine how the difference in electron-blocking capacity affects PLED device response. To evaluate the electron-blocking properties of PEDOT-PSS and the $TPDSi_2$ + TFB blend, we fabricated electron-dominated PLEDs with BT as the EML and Ca as the cathode (Figures 8). BT has excellent electron transport but weak hole-transport capacity (Figure 3), and in a BT/Ca-based device, there should be a significant electron flux reaching the HTL/BT interface, which renders it an ideal model structure to investigate electron-blocking characteristics at the HTL/BT interface.

The only obvious difference between device 3 (ITO/PEDOT-PSS/$TPDSi_2$ + TFB blend/BT/Ca/Al) and device 4 (ITO/PEDOT-PSS/BT/Ca/Al) is the presence of a thin $TPDSi_2$ + TFB blend layer between the PEDOT-PSS and BT layers. As seen in Figure 8, the 10-fold enhancement in current efficiency and lesser total current flow for device 3 must reflect the pronounced electron-blocking characteristics of the $TPDSi_2$ + TFB blend at the $TPDSi_2$ + TFB/BT interface. Therefore, in device 4, a significant electron flux must simply pass through the BT layer without encountering/recombining with holes and is then simply drained unproductively to the ITO anode through the highly conductive PEDOT-PSS HTL, leading to lower hole-electron recombination efficiency and, hence, lower device current efficiency. Clearly, the $TPDSi_2$ + TFB blend exhibits significantly greater electron-blocking properties than a conventional PEDOT-PSS HTL, and PLED performance can be dramatically enhanced by depositing a thin $TPDSi_2$ + TFB blend electron-blocking interlayer onto the PEDOT-PSS HTL.

Leakage Currents of BT-Based Devices Fabricated on Films 1, 2, 3, 4, and 5. Another important function of a PLED HTL is planarizing the ITO anode surface, to prevent local shorting currents, and to thus improve device performance and uniformity of performance. The commercial ITO source used in the present study has an RMS roughness of 3.0−4.0 nm by contact-mode AFM, and spikes as high as 20 nm can be

(54) Morgado, J.; Friend, R. H.; Cacialli, F. *Appl. Phys. Lett.* **2002**, *80*, 2436−2438.

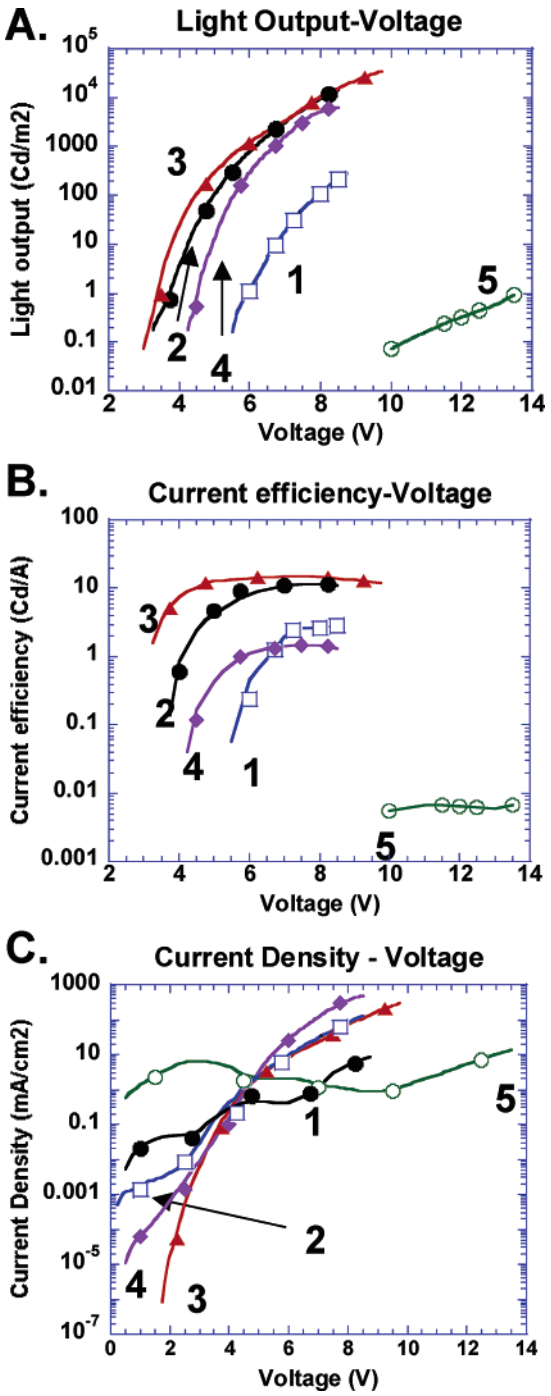

Figure 8. (A) Light output; (B) current efficiency; (C) I−V characteristics as a function driving voltage for devices having the structure ITO/ HTL/ BT/Ca/Al. The HTLs compared are: (1, 0) $TPDSi_2$ SAM; (2, b) the blend HTL; (3, 2) the double layer HTL; (4,]) PEDOT-PSS; (5, O) bare ITO. Lines through the data points are drawn as a guide to the eye.

occasionally observed on the surface by AFM. For the present series of electron-dominated PLED devices using BT as the EML (Figure 8), there should be a significant electron flux reaching the HTL/BT interface, which can serve to magnify the anode/HTL-mediated leakage currents. Therefore, the present BT-based PLED series represents a good model system in which to investigate leakage current levels and planarization effects associated with the various HTLs. As seen in Figure 8, when bare ITO is used as the anode, the BT-based device on 5 (ITO/ BT/Ca/Al) supports a substantial leakage current density of ∼1 mA/cm^2. The ability of the $TPDSi_2$ SAM hydrophobic structure to exclude moisture[52] likely plays a role in reducing leakage currents in the BT-based devices on 1 (ITO/$TPDSi_2$ SAM/BT/ Ca/Al). However, while the thin $TPDSi_2$ SAM only provides conformal monolayer coverage on the ITO surface, it has no discernible planarization effects (RMS roughness = 3.9 nm). Therefore, there is reduced but still significant leakage current density (0.01−0.1 mA/cm^2) in the $TPDSi_2$ SAM/BT-based devices vs bare ITO. The spin-coated $TPDSi_2$ + TFB blend can also planarize the ITO surface (RMS roughness reduced to 1.7 nm), which leads to greater reduction in device leakage current density (to 0.001−0.01mA/cm^2). We suspect that the $TPDSi_2$ + TFB blend coating (thickness ∼10−15 nm) is insufficient to fully cover the ITO surface spikes. In contrast, the double-layer HTL (PEDOT-PSS/$TPDSi_2$ + TFB blend) has a thickness of ∼60 nm and can planarize the ITO surface more effectively (RMS roughness now ∼1 nm), which is consistent with the observed negligible leakage current densities (current at 2 V ∼0.00001mA/cm^2, which is comparable to the uncertainly limits of the instrumentation) in device 3 of Figure 8.

Why the Double-Layer HTL (ITO/PEDOT-PSS/$TPDSi_2$ + TFB Blend) Devices Exhibit the Highest Performance. In the following discussion, we will analyze the response characteristics of the double-layer HTL-based devices vs those based on a $TPDSi_2$ SAM alone, the blend HTL, and PEDOT-PSS from three perspectives: (1) hole-injection capacity (studied using hole-only devices); (2) electron-blocking capacity (studied by BT-based electron-dominated PLED devices); (3) anode planarization effects and leakage current densities.

The Double-Layer HTL vs $TPDSi_2$ SAMs. As shown in Figure 7, the double-layer HTL provides slightly greater hole-injection capacity compared to the $TPDSi_2$ SAM. This alone cannot explain the difference in device efficiency of the corresponding PLED devices in Figure 6B (current efficiency, 17 vs 6 cd/A). The $TPDSi_2$ structure should be electron-blocking, however, there is a question as to whether the ultrathin $TPDSi_2$ SAM is sufficiently thick to effectively block the overflow of electrons. As can be seen in Figure 8B, the maximum current efficiency of the $TPDSi_2$ SAM-based BT device is only ∼20% of that of the double-layer HTL-based device. This probably indicates that the electron-blocking capacity of the $TPDSi_2$ SAM is significantly weaker than that of the double-layer HTL. In addition, as can be seen in Figure 8A, the turn-on voltage of the $TPDSi_2$ SAM and the double-layer HTL-based devices are 5.5 and 3.1 V, respectively. It is widely recognized[32,54,55] that electron density build-up at the HTL/EML interface can enhance anode hole injection at lower fields, and as a result, devices with a greater electron-blocking capacity at the HTL/EML interface should exhibit lower turn-on voltages. Therefore, the significantly greater turn-on voltage of the $TPDSi_2$ SAM-based device further supports the contention that the $TPDSi_2$ SAM has weaker electron-blocking capacity than the double-layer HTL. Finally, as shown in Figure 8C, the $TPDSi_2$ SAM-based device exhibits 1000-fold greater leakage current than the double-layer HTL-based device at 2 V, which is probably due to the lack of $TPDSi_2$ SAM planarizing effects on the ITO surface. As discussed by Tutis et al.,[56] charge

(55) Murata, K.; Cina, S.; Greenham, N. C. *Appl. Phys. Lett.* **2001**, *79*, 1193−1195.
(56) Tutis, E.; Bussac, M. N.; Zuppiroli, L. *Appl. Phys. Lett.* **1999**, *75*, 3880−3882.

Table 2. Comparison of $TPDSi_2$ SAM, the Blend HTL, the Double-Layer HTL, and PEDOT-PSS Features for PLED Fabrication

	PEDOT-PSS	1, $TPDSi_2$ SAM	2, blend HTL	3, double-layer HTL
thickness (nm)	45	1.8	15	60
RMS roughness (nm)	1.1	3.9	1.7	1.0
ITO planarization	better	no	good	best
hole injection	good	good	good	good
electron-blocking	no	no	good	best
maximum current efficiency (Cd/A)	10	6.0	14	17
turn-on voltage (V)	2.0	2.5	2.0	2.0
notes	poor electron-blocking	interfacial modification; hole injection	cross-linked network; flexibility; HTL/EML HOMO alignment	electron-blocking; new rationale for PLED design

tunneling and image forces can be present at length scales of ~1 nm, which is comparable to the width of the electron-blocking triarylamine core structure of the $TPDSi_2$ SAM, leading to possible electron tunneling through the ultrathin $TPDSi_2$ SAM. To conclude, although the $TPDSi_2$ SAM structure is electron-blocking, it appears to be too thin to provide optimum electron blocking or to prevent local leakage currents, which is also the reason the double-layer HTL-based PLED exhibits superior performance.

The Double-Layer HTL vs the Blend HTL. As shown in Figure 7, the hole-injection capacities of the double-layer HTL and the blend HTL are comparable. Note from Figure 8, however, that the double-layer HTL-based device still exhibits 50% greater current efficiency and 0.4 V lower turn-on voltage vs the blend HTL-based device, which suggests a slightly weaker electron-blocking capacity for the blend HTL. It is suspected that the blend HTL (thickness ~10−15 nm) is not sufficiently thick to fully cover the ITO surface, especially occasional spikes, which could introduce significant leakage current density and may adversely affect the electron-blocking properties. AFM analysis of the ITO/$TPDSi_2$ + TFB films verify this point: ITO-originated surface spikes are significantly reduced with the $TPDSi_2$ + TFB coating but can still be occasionally observed.

The Double-Layer HTL vs PEDOT-PSS. As discussed before, for the BT-based electron-dominated device series, the double-layer HTL device exhibits ~10-fold greater current efficiency than does the PEDOT-PSS device due to the excellent electron-blocking properties of the former. In addition, other factors may also play important roles. As noted above, PEDOT-PSS has been shown to mediate polyfluorene EML oxidative doping, leading to reduced luminous efficiency.[23] For the present double-layer HTL, since TFB is commonly used as the hole-transporting component in EML blends[57] and $TPDSi_2$ consists of stable, neutrally-charged siloxane and arylamine moieties, both components should not introduce luminescence quenching as does PEDOT-PSS.[23] Therefore, the present double-layer HTL may reduce PEDOT-PSS-induced luminescence quenching by separating the PEDOT-PSS layer from the EML.

As shown in Figure 6, for the TFB + BT-based device series in which the EML has balanced charge transport, the double-layer HTL still provides significantly greater device performance than PEDOT-PSS (current efficiency = 17 vs 10 cd/A). The reason for this appears to be that, although TFB + BT has balanced electron and hole transport, there is still a non-negligible electron flow reaching the PEDOT-PSS HTL/EML interface without recombining with holes in device 4, thus resulting in lower recombination efficiency and hence lower luminous efficiency. The reduced PEDOT-PSS-induced luminescence quenching by the double-layer HTL may also play a role here.

Comparison of the $TPDSi_2$ SAM, the $TPDSi_2$ + TFB Blend HTL, and the Double-Layer HTL vs PEDOT-PSS. The important features of the present devices based on the $TPDSi_2$ SAM, the blend HTL, the double-layer HTL, and PEDOT-PSS are summarized in Table 2. The 17 cd/A current efficiency of the double-layer HTL-based devices is one of the highest PLED current efficiencies reported to date. With further materials and device structure refinement, additional improvements can be expected. In addition, the present double-layer HTL approach offers many other attractions: (1) convenience, cross-linking of the $TPDSi_2$ + TFB blend is complete within seconds after spin-coating in air at room temperature, with no special high-temperature baking, photo,[26] or thermal cross-linking[24,28] required; (2) flexibility, siloxane materials other than $TPDSi_2$ and polymers other than TFB should also be applicable; future siloxanes or polymers having greater hole-transporting and/or electron-blocking capacity should yield even more effective hole-transporting and electron-blocking layers and greater PLED performance; (3) energetic tuning, PLED energy level matching should be readily tunable by using a hole-transporting polymer that matches an EML HOMO level. In this contribution, TFB is the hole-transporting component of both the HTL and EML device components. Thus, hole transport from the HTL to the EML can propagate through the same TFB structure, with near-perfect HTL-EML HOMO level alignment. Therefore, the present approach can be used as a general strategy to manipulate PLED HTL-EML HOMO level alignment.

Comparison of the $TPDSi_2$ + TFB Blend with PPV as Electron-Blocking Layers. In the recent work by Morgado et. al., [54] upon insertion of a PPV electron-confinement layer between a PEDOT-PSS HTL and a fluorene-based EML, the current density in the PLED device was reduced by ~ 20%, and the maximum current efficiency was nearly doubled. In that study, the EML was a blend of poly(9,9-dioctylfluorene) (PFO) and BT, which is a balanced-charge-transporting EML. The reduced current density observed may be partially due to the 10-fold lower hole mobility of PPV[54] compared with that of PFO. However, the current reduction alone is not enough to explain the doubling of current efficiency. The authors suggested that the largest contribution to the efficiency increase comes from the electron-blocking effect at the PPV/EML interface.

(57) Cina, S.; Baynes, N.; Moons, E.; Friend, R. H.; Burroughes, J. H.; Towns, C.; Heeks, K.; O'Dell, R.; O'Connor, S.; Athanassopoulou, N. *Proc. SPIE* **2001**, *4279*, 221−228.

This result suggests that PEDOT-PSS HTLs might not possess as great electron-blocking capacity as PPV.

In our study, instead of using EMLs with balanced charge transport as in Morgado's work, we chose an electron-dominated EML, BT, to fabricate an electron-dominated PLED structure, PEDOT-PSS/BT/Ca, in which there are sizable electron currents reaching the PEDOT-PSS/BT interface and electron-blocking effects at interface can be readily studied. By use of this model structure, we find that the insertion of a $TPDSi_2$ + TFB EBL between the PEDOT-PSS HTL and the BT EML leads to ~15-fold increase in PLED device current efficiency and 2-fold decrease in current density, clearly a result of effective electron-blocking at the HTL/EML interface. The result also shows that PEDOT-PSS HTLs possess significantly weaker electron-blocking capacity than the $TPDSi_2$ + TFB blend.

The present $TPDSi_2$ + TFB blend offers other significant attractions vs PPV as an EBL: (1) $TPDSi_2$ + TFB blends should have a hole mobility comparable to PFO or TFB[58,59] and do not suppress PLED anode hole injection, as supported by the hole-only device data (Figure 7). In contrast, PPV has lower hole mobility[54] than most polyfluorene EMLs, which may reduce hole injection in the device and increase the device operating voltage. (2) $TPDSi_2$ + TFB blends at most only exhibit weak luminescence in blue region and should be less likely to interfere with EML light emission than should PPV, a well-known efficient yellow-green-emitting polymer. (3) Fabrication of $TPDSi_2$ + TFB blends is convenient. As noted above, $TPDSi_2$ + TFB blend cross-linking is complete within seconds after spin-coating in air at room temperature, with no special high-temperature curing, photo,[26] or thermal cross-linking[24,28] required. However, fabrication of an insoluble PPV layer involves the spin-coating of a PPV precursor followed by high-temperature (200−300 °C) in situ polymerization. The resulting PPV layer is not covalently linked to the anode surface in any obvious way. (4) PPV has LUMO energy of ~2.7 eV; however, the LUMO energy of the $TPDSi_2$ + TFB blend is ~2.3 eV (Figure 3), which is at least 0.5 eV smaller than typical EML LUMO values (2.8−3.1 eV) and should therefore give rise to greater electron-blocking capacity vs PPV.

Relevance of the Present Siloxane HTL Approach to Generalizable PLED Fabrication Strategies. The consequences of the present siloxane HTL approach lie in two areas. First, the results show for the first time that high-performance PLEDs can be achieved using an electron-dominated EML. For a conventional PLED device, in which p-doped conducting polymers (e.g., PEDOT-PSS) are usually employed as the HTL, it has been necessary for the EML to have balanced hole and electron transports to achieve superior PLED performance, and the choice of a high-performance PLED EML has to date been quite limited. Many unipolar emissive polymers (electron-dominated or hole-dominated), despite their impressive luminescence properties, yield poor PLED device performance and have been regarded as unsuitable for PLED EML applications. An example of such an electron-dominated EML material is BT, which has excellent electroluminescent properties but highly electron dominant transport capacity. As a result, PLEDs using BT as the EML and PEDOT-PSS as the HTL usually exhibit poor device performance (current efficiency 1−2 cd/A[55]). In our study, however, it is shown that BT-based PLEDs can exhibit excellent performance when the conventional PEDOT-PSS HTL is replaced with a cross-linked siloxane-based HTL that has greater electron-blocking capacity. This result indicates that the marginal performance of PEDOT-PSS/BT/Ca-based devices is caused by the insufficient electron-blocking capacity of the PEDOT-PSS HTL instead of the unipolar charge transport properties of BT. By employing an electron-blocking HTL in a PLED structure, the choice of PLED EML is no longer limited to balanced-charge-transporting emissive polymers, and consequently, there should be far greater flexibility for further development and optimization of PLED EMLs.

In addition, the performance of PLEDs based on an electron-dominated EML (BT) and an electron-blocking HTL (the $TPDSi_2$ + TFB-based double-layer HTL) reported here (current efficiency = 17 cd/A) significantly surpasses that of PLEDs based on a TFB + BT blend EML (TFB + BT blends are known to exhibit better balanced electron−hole transport than the BT-only EML) and a PEDOT-PSS HTL (current efficiency = 10 cd/A). This 17 cd/A efficiency is also comparable with previously reported PLEDs[60] with a molecularly engineered HTL and a different BT-based blend EML. This result can be rationalized by the following. In the PEDOT-PSS/TFB + BT-based device, although TFB + BT has better balanced electron and hole transport, there is likely to be a nonnegligible electron flux that reaches the HTL/EML interface and is drained with recombination to the anode, leading to lower luminous efficiency. Furthermore, the peak recombination zone of such devices should be located near the middle part of the TFB + BT EML, and the distance between the peak recombination zone and the cathode or the PEDOT-PSS HTL should be ~35 nm, which may lead to considerable cathode or PEDOT-PSS-induced luminescence quenching. For the $TPDSi_2$ + TFB/BT-based device, however, the peak recombination zone should be located near the $TPDSi_2$ + TFB/BT interface which is ~70 nm away from the cathode, leading to less cathode-induced luminescence quenching. Also, the $TPDSi_2$ + TFB layer should not quench luminescence as does the PEDOT-PSS HTL since its triarylamine core structure is widely used in PLED EML components. Therefore, among the two approaches to design PLEDs (PLEDs having an electron-dominated EML and an electron-blocking HTL or PLEDs having a charge balanced EML and a conventional HTL), the former appears to be able to afford significantly greater PLED performance. More fundamentally, this study shows that developing new HTLs and optimizing HTL electron-blocking properties may be a more productive approach to achieving high-performance PLEDs than merely manipulating the charge transport properties of the EML. (Previous research on small molecule OLEDs and PLEDs has demonstrated that molecular-level engineering[60] and tuning of electron-blocking capacity[1] of the HTL are important issues for OLEDs or PLEDs; our results offer a convenient approach to achieving easy tunability of the electron-blocking capacity of PLED HTLs.)

(58) Redecker, M.; Bassler, H.; Horhold, H. H. *J. Phys. Chem. B* **1997**, *101*, 7398−7403.
(59) Redecker, M.; Bradley, D. D. C.; Inbasekaran, M.; Wu, W. W.; Woo, E. P. *Adv. Mater.* **1999**, *11*, 241−246.
(60) Ho, P. K. H.; Kim, J. S.; Burroughes, J. H.; Becker, H.; Y.Li, S. F.; Brown, T. M.; Cacialli, F.; Friend, R. H. *Nature* **2000**, *404*, 481−484.
(61) Campbell, A. J.; Bradley, D. C. C.; Antoniadis, H. *J. Appl. Phys.* **2001**, *89*, 3343−3351.
(62) Cui, J.; Wang, A.; Edleman, N. L.; Ni, J.; Lee, P.; Armstrong, N. R.; Marks, T. J. *Adv. Mater.* **2001**, *13*, 1476.

V. Conclusions

We have developed cross-linkable hole-transporting and electron-blocking organosiloxane materials such as $TPDSi_2$ as effective components for PLED HTLs. By utilization of the chemical reactivity of $TPDSi_2$ with respect to ITO surfaces together with its self-cross-linking ability, three types of PLED HTLs have been developed. First, $TPDSi_2$ can be chemisorbed onto ITO to form a self-assembled monolayer (SAM). $TPDSi_2$ SAM modification can increase the work function of ITO, change ITO surface hydrophilicity, enhance anode-transport layer cohesion, enhance ITO anode hole injection, and hence improve PLED performance. Second, $TPDSi_2$ can be blended with a hole-transporting polymer (TFB) and spin-coated onto ITO to form an insoluble cross-linked blend network that can be employed as a PLED HTL. Covalent chemical bonding of $TPDSi_2$ to the ITO anode facilitates hole injection from the ITO into the HTL and enhances device durability. The present $TPDSi_2$ + TFB blend is also shown to have greater electron-blocking capacity compared to PEDOT-PSS, which appears to be the reason for the 10-fold enhancement in current efficiency of the BT-based electron-dominated PLEDs. Finally, the $TPDSi_2$ + TFB blend can be deposited on PEDOT-PSS-coated ITO to form a double-layer HTL. This double-layer HTL can most effectively planarize the ITO surface and minimize device leakage currents. Simultaneously, it has impressive hole-injection and electron-blocking capacities, all of which combine to afford excellent PLED performance with maximum current efficiencies as high as 17 cd/A, maximum luminance as high as 140 000 cd/m^2, and turn-on voltage as low as 2 V. The present organosiloxane approach to fabricating PLED HTLs offers many other attractions such as ease of fabrication, flexibility in choosing HTL components, and reduced PEDOT-PSS-induced EML luminescence quenching and can be applied as an important strategy to achieve high-performance PLEDs.

Acknowledgment. We thank the U. S. Display Consortium and the NSF-MRSEC program through the Northwestern Materials Research Center (DMR-0076097) for support of this research.

JA044455Q